Bounding Integrity Risk in the Presence of Parametric Time Correlation Uncertainty

Steven Langel, Samer Khanafseh and Boris Pervan
Illinois Institute of Technology, Chicago, IL

ABSTRACT

State estimation of linear dynamical systems with time correlation uncertainty in the measurement noise is considered. The presence of random noise introduces a state estimate error that is defined in terms of a probability distribution. For safety-of-life aviation applications, the integrity risk associated with the state estimate error must be explicitly quantified. This paper focuses on developing a methodology to compute upper bounds on integrity risk subject to a parametric uncertainty structure on the measurement noise autocorrelation function.

Using well known results from linear algebra, we derive a concise formula which describes how the autocorrelation uncertainty maps from the measurement domain to the position domain. This formula allows the integrity risk to be written directly in terms of the unknown parameters. For autocorrelation functions described by a 1st order Gauss-Markov model, the integrity risk bounding problem is formulated as a polynomial optimization problem with non-linear inequality constraints. An efficient numerical algorithm is developed to obtain the global optimum, hence guaranteeing that the computed integrity risk will always upper bound the true risk.

INTRODUCTION

For applications where the unknown state evolves according to a dynamic model, measurements are typically processed (or filtered) over time. It is generally recognized that GPS measurement errors are time-correlated due to the presence of multipath which must be properly accounted for in the estimation algorithm. In practice, multipath is usually modeled as a 1st order Gauss-Markov process which is completely specified in terms of a variance and time constant. However, the precise value of these parameters is rarely available. For high integrity aviation applications like the Navy's Unmanned Combat Air System (N-UCAS) or the Joint Precision Approach and Landing System (JPALS), it is absolutely essential to determine how this uncertainty affects the computed integrity risk.

In the GPS community, an abundance of research has addressed the issue of uncertainty in characterizing the measurement noise. Using the concept of CDF overbounding, DeCleene [1] showed how to compute a conservative integrity risk under the assumption that the measurement noise is independent with a distribution that is zero-mean, symmetric and unimodal. This result was generalized to arbitrary measurement noise distributions by Rife using the paired overbounding theorem [2]. However, the theorem still rests on the assumption that the measurement noise is independent. Although justified for snapshot positioning algorithms, this assumption is not appropriate for applications involving measurement filtering due to the presence of time-correlated multipath error.

When the measurement noise also contains an uncertain correlation structure, the problem of ensuring integrity becomes especially difficult. DeCleene and Rife were able to derive their results using arguments based on convolution, which is permitted under the independence assumption. Once the measurement noise is allowed to be correlated, these arguments break down and a new approach must be developed to bound the integrity risk. Rife et al [3] used the concept of spherical symmetry as the framework for treating correlated measurement errors, ultimately resulting in the symmetric overbounding theorem. Pulford [4] provided an alternative derivation that formulates the overbound in terms of state space matrices. This theorem provides the necessary theoretical

foundation for ensuring integrity in the presence of correlated measurement noise.

Others have taken a more practical approach by considering specialized cases of time correlation uncertainty. For example, Khanafseh et al [5] assume that the measurement noise is governed by a 1st order Gauss-Markov process with known variance. However, the time constant is only known to lie within a given interval. One of the key results in [5] is the assertion that is impossible to bound the integrity risk using a single value of the time constant and they propose a solution using a bank of Kalman filters.

In this paper, we investigate the more general version of the problem considered in [5] where both the variance and time constant are unknown. Using a new derivation of the state estimate error, an upper bound on the integrity risk is computed for batch weighted least squares (WLS) estimators. These algorithms are simulated numerically for the benchmark application of autonomous shipboard landing. Emphasis is placed on determining the impact of uncertainty in the variance and time constant on the vertical fault-free integrity risk.

FUNDAMENTALS OF INTEGRITY RISK

Fault-free integrity risk is defined as the probability of the relative position estimate error vector residing outside a specified region, A.

$$I_0 = P\left(\boldsymbol{\varepsilon}_{\Delta x} \notin A\right) \tag{1}$$

where I_0 is the fault-free integrity risk and $\boldsymbol{\varepsilon}_{\Delta x}$ is defined as

$$\boldsymbol{\varepsilon}_{\Delta x} = \Delta\hat{\boldsymbol{x}} - \Delta\boldsymbol{x} \tag{2}$$

where $\Delta\hat{\boldsymbol{x}}$ is an estimate of the relative position vector, $\Delta\boldsymbol{x}$.

In aviation, A is usually defined separately for certain linear combinations of the components of $\boldsymbol{\varepsilon}_{\Delta x}$.

$$I_{0,\eta} = P\left(\varepsilon_\eta \notin \left[-a_\eta, a_\eta\right]\right) \tag{3}$$

where ε_η is a scalar linear combination of the components of $\boldsymbol{\varepsilon}_{\Delta x}$ and a_η is a given alert limit.

For example, ε_η may be the vertical component of $\boldsymbol{\varepsilon}_{\Delta x}$ with a_η being the corresponding vertical alert limit.

Assuming that ε_η is a zero-mean Gaussian random variable, $I_{0,\eta}$ can readily be expressed in the form

$$I_{0,\eta} = \operatorname{erfc}\left(\frac{a_\eta}{\sqrt{2\sigma_\eta^2}}\right) \tag{4}$$

where $\operatorname{erfc}(\bullet)$ is the complementary error function and σ_η^2 is the variance of ε_η.

To illustrate how σ_η^2 is obtained, consider the weighted least squares (WLS) estimator for the linear measurement model

$$\boldsymbol{z} = \mathbf{H}\boldsymbol{x} + \mathbf{J}\boldsymbol{\nu} \tag{5}$$

where $\boldsymbol{z}$ is the measurement vector, $\mathbf{H}$ is the observation matrix, $\boldsymbol{x}$ is the state vector of which $\Delta\boldsymbol{x}$ is a subset, $\mathbf{J}$ is the measurement noise mapping matrix and $\boldsymbol{\nu}$ is a zero-mean Gaussian random noise vector with covariance matrix $\mathbf{P}_\nu$.

The WLS estimate of $\boldsymbol{x}$ and the associated estimate error vector are given by [6]

$$\hat{\boldsymbol{x}} = \mathbf{S}\boldsymbol{z} \tag{6}$$

$$\boldsymbol{\varepsilon} = \hat{\boldsymbol{x}} - \boldsymbol{x} = \mathbf{S}\mathbf{J}\boldsymbol{\nu} \tag{7}$$

where $\mathbf{S}$ is the weighted left pseudo-inverse of $\mathbf{H}$ with weighting matrix $\mathbf{W} = \mathbf{J}\mathbf{P}_\nu\mathbf{J}^T$.

$$\mathbf{S} = \left[\mathbf{H}^T\left(\mathbf{J}\mathbf{P}_\nu\mathbf{J}^T\right)^{-1}\mathbf{H}\right]^{-1}\mathbf{H}^T\left(\mathbf{J}\mathbf{P}_\nu\mathbf{J}^T\right)^{-1} \tag{8}$$

The random variable ε_η is obtained from $\boldsymbol{\varepsilon}$ through the linear transformation

$$\varepsilon_\eta = \boldsymbol{\alpha}_\eta^T\boldsymbol{\varepsilon} \tag{9}$$

where $\boldsymbol{\alpha}_\eta^T$ is a known vector.

Substituting equation (7) into equation (9) and taking the expected value of ε_η^2 yields the following expression for σ_η^2.

$$\sigma_\eta^2 = \boldsymbol{\alpha}_\eta^T \mathbf{S}\mathbf{J}\mathbf{P}_\nu \mathbf{J}^T \mathbf{S}^T \boldsymbol{\alpha}_\eta \tag{10}$$

Equation (10) clearly shows that σ_η^2 is directly related to $\mathbf{P}_\nu$. Therefore, $\mathbf{P}_\nu$ must be perfectly known in order for equation (4) to provide accurate values of $I_{0,\eta}$. If $\mathbf{P}_\nu$ cannot be specified exactly, then it must be approximated in such a way that σ_η^2 is always inflated relative to its true value. This will guarantee that $I_{0,\eta}$ always provides a conservative assessment of the fault-free integrity risk.

FIRST ORDER GAUSS-MARKOV MODEL

In general, the measurement noise covariance matrix $\mathbf{P}_\nu$ is only required to be a symmetric, positive semi-definite matrix. For measurements collected over time from a single sensor, the elements of $\mathbf{P}_\nu$ are defined as

$$\left(\mathbf{P}_\nu\right)_{ij} = E\left[\nu_i \nu_j\right] \quad , \quad \begin{matrix} i = 1, 2, \cdots, N \\ j = 1, 2, \cdots, N \end{matrix} \tag{11}$$

where E is the expectation operator, ν_i and ν_j are measurement noise samples at times i and j, respectively, and N is the total number of noise samples.

The diagonal elements of $\mathbf{P}_\nu$ represent the noise variance and the off-diagonal elements capture the correlation between noise samples.

In practice, a mathematical model is typically formulated which allows the expected values in equation (11) to be computed in terms of a small handful of parameters. One model that is used quite often is the first order Gauss-Markov model, which has an exponential autocorrelation function [7]

$$E\left[\nu_i \nu_j\right] = r_0 \exp\left(-\frac{|i-j|\,T}{\tau}\right) \tag{12}$$

where r_0 is the measurement noise variance, T is the sampling interval of the sensor and τ is the time constant of the Gauss-Markov process.

As long as r_0 and τ are known, equation (12) can be used to populate $\mathbf{P}_\nu$. If these parameters are unknown, how should they be chosen so that σ_η^2 always upper bounds the true estimate error variance? The long held belief is that measurements with highly correlated errors do not contain as much information as those with less correlated errors, and therefore larger time constants should always produce a conservative integrity risk. After all, this is precisely the conclusion that is reached when considering bias estimation. However, as we'll see later on, this is not always true and a more mathematically rigorous approach must be taken to address the issue of time-correlation uncertainty.

INTEGRITY RISK WITH MODELING UNCERTAINTY

In the linear model of equation (5), assume that $\mathbf{H}$ and $\mathbf{J}$ are known but only an approximate measurement noise covariance matrix $\hat{\mathbf{P}}_\nu$ is available. Then the matrix $\mathbf{S}$ shown in equation (8) which defines the WLS estimator must be replaced by its approximation $\hat{\mathbf{S}}$. Making this change in equation (10) yields the following expression for σ_η^2.

$$\sigma_\eta^2 = \boldsymbol{\alpha}_\eta^T \hat{\mathbf{S}}\mathbf{J}\mathbf{P}_\nu \mathbf{J}^T \hat{\mathbf{S}}^T \boldsymbol{\alpha}_\eta \tag{13}$$

Notice that the $\mathbf{P}_\nu$ appearing in the middle of equation (13) has not been changed to $\hat{\mathbf{P}}_\nu$. Making this change would simply produce an equation for σ_η^2 under the assumption that $\mathbf{P}_\nu = \hat{\mathbf{P}}_\nu$. Therefore, equation (13) accurately reflects the fact that the WLS estimator is using $\hat{\mathbf{P}}_\nu$ as an approximation to the unknown matrix $\mathbf{P}_\nu$.

Given that $\mathbf{P}_\nu$ depends on r_0 and τ, an upper bound on σ_η^2 must be obtained for all permissible parameter values in order to ensure integrity. One approach to solving this problem is to perform the matrix multiplication in equation (13) and extract an expression for σ_η^2 in terms of r_0 and τ. After completing this tedious process, it was discovered that the same result could be obtained using known results from linear algebra.

For an arbitrary vector $\boldsymbol{y}$ and an arbitrary square matrix $\mathbf{A}$, the quadratic form $\boldsymbol{y}^T \mathbf{A}\, \boldsymbol{y}$ can be written as [8]

$$\boldsymbol{y}^T \mathbf{A} \boldsymbol{y} = \sum_{ij} \left[\left(\boldsymbol{y} \boldsymbol{y}^T \right) \circ \mathbf{A}^T \right]_{ij} \tag{14}$$

where the symbol $\circ$ indicates the entry-wise product of two matrices, defined as [8]

$$\left(\mathbf{A} \circ \mathbf{B} \right)_{ij} = a_{ij} b_{ij} \tag{15}$$

Applying equation (14) to equation (13) with $\mathbf{A} = \mathbf{P}_\nu$ and $\boldsymbol{y} = \mathbf{J}^T \hat{\mathbf{S}}^T \boldsymbol{\alpha}_\eta$ yields

$$\sigma_\eta^2 = \sum_{ij} \left[\left(\mathbf{J}^T \hat{\mathbf{S}}^T \boldsymbol{\alpha}_\eta \boldsymbol{\alpha}_\eta^T \hat{\mathbf{S}} \mathbf{J} \right) \circ \mathbf{P}_\nu^T \right]_{ij} \tag{16}$$

which can also be written as

$$\sigma_\eta^2 = \sum_{ij} \left(\mathbf{D} \circ \mathbf{P}_\nu \right)_{ij} \tag{17}$$

where $\mathbf{D} = \mathbf{J}^T \hat{\mathbf{S}}^T \boldsymbol{\alpha}_\eta \boldsymbol{\alpha}_\eta^T \hat{\mathbf{S}} \mathbf{J}$ and we have used the fact that $\mathbf{P}_\nu$ is a symmetric matrix.

In the previous section on the Gauss-Markov model, the elements of $\mathbf{P}_\nu$ were defined for measurements collected over time from a single sensor. However, measurements are generally available over time from *M* sensors, leading to the following form for $\boldsymbol{\nu}$

$$\boldsymbol{\nu} = \begin{bmatrix} \boldsymbol{\nu}_1^T & \boldsymbol{\nu}_2^T & \cdots & \boldsymbol{\nu}_M^T \end{bmatrix}^T \tag{18}$$

where each $\boldsymbol{\nu}_m$ represents a time series of the measurement noise from sensor *m*. If *N* measurements are available from each sensor, then $\boldsymbol{\nu}_m$ is given by

$$\boldsymbol{\nu}_m = \begin{bmatrix} \nu_{m,1} & \nu_{m,2} & \cdots & \nu_{m,N} \end{bmatrix}^T \tag{19}$$

Assuming that measurement errors are uncorrelated across sensors, $\mathbf{P}_\nu$ is a block diagonal matrix

$$\mathbf{P}_\nu = E\left[\boldsymbol{\nu} \boldsymbol{\nu}^T \right] = \begin{bmatrix} \mathbf{P}_{\nu,1} & \mathbf{0} & \cdots & \mathbf{0} \\ \mathbf{0} & \mathbf{P}_{\nu,2} & \cdots & \mathbf{0} \\ \vdots & \vdots & \ddots & \vdots \\ \mathbf{0} & \mathbf{0} & \cdots & \mathbf{P}_{\nu,M} \end{bmatrix} \tag{20}$$

This block diagonal structure can be exploited to express equation (17) as

$$\sigma_\eta^2 = \sum_{m=1}^{M} \sum_{ij} \left[\mathbf{D}_m \circ \mathbf{P}_{\nu,m} \right]_{ij} \tag{21}$$

where $\mathbf{D}_m$ is the m^{th} diagonal block of $\mathbf{D}$.

Making the following change of variables in equation (12)

$$\xi_m = \exp\left(-\frac{T}{\tau_m} \right) \tag{22}$$

results in a matrix $\mathbf{P}_{\nu,m}$ with the following symmetric Toeplitz structure

$$\mathbf{P}_{\nu,m} = r_{0,m} \begin{bmatrix} 1 & \xi_m & \xi_m^2 & \cdots & \xi_m^{N-1} \\ \xi_m & 1 & \xi_m & \ddots & \vdots \\ \xi_m^2 & \xi_m & \ddots & \ddots & \xi_m^2 \\ \vdots & \ddots & \ddots & 1 & \xi_m \\ \xi_m^{N-1} & \cdots & \xi_m^2 & \xi_m & 1 \end{bmatrix} \tag{23}$$

Substituting equation (23) into equation (21) and using the definition of the entry-wise product given in equation (15) yields the following expression for σ_η^2.

$$\sigma_\eta^2 = \sum_{m=1}^{M} r_{0,m} \left(s_{0,m} + 2 \sum_{k=1}^{N-1} s_{k,m} \xi_m^k \right) \tag{24}$$

where $s_{k,m}$ is the sum of the elements along the k^{th} diagonal of $\mathbf{D}_m$.

Equation (24) expresses σ_η^2 as a sum of *M* polynomials in the unknown variables $r_{0,m}$ and ξ_m. Before describing a procedure for upper bounding σ_η^2, it is necessary to define an uncertainty structure for $r_{0,m}$ and ξ_m.

GAUSS-MARKOV UNCERTAINTY MODEL

The Gauss-Markov model is actually a model of the sensor error autocorrelation function, $r_{k,m}$. In this work, $r_{k,m}$ is known to lie between two exponential bounding functions.

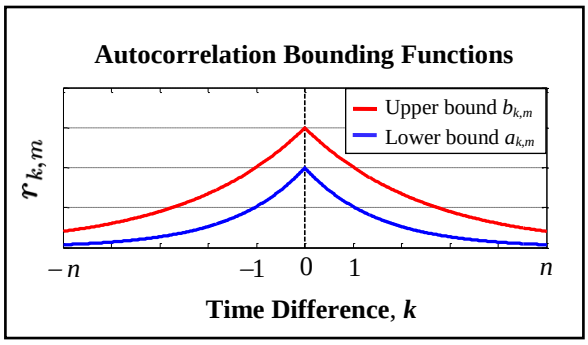

Figure 1: Autocorrelation uncertainty structure

Exponential bounding functions are used in this work because the measurement noise is known to be exponentially correlated. Furthermore, notice from figure 1 that the autocorrelation function has only been bounded up to time shifts of n, where $n = N - 1$. Given that N measurements are available from a particular sensor, time shifts beyond $N - 1$ do not impact the integrity risk computation. Hence, it is not necessary to bound the autocorrelation function beyond time shifts of $N - 1$.

Any candidate autocorrelation function that lies between these two bounding functions must satisfy the following constraints

$$a_{0,m} \le r_{0,m} \le b_{0,m} \tag{25}$$

$$a_{n,m} \le r_{0,m}\,\xi_m^n \le b_{n,m} \tag{26}$$

where $a_{0,m}$ and $a_{n,m}$ are the values of the lower bounding function at $k = 0$ and $k = n$, respectively. The variables $b_{0,m}$ and $b_{n,m}$ are similarly defined for the upper bounding function.

The fact that these two boundary conditions ensure that $r_{k,m}$ will never cross the bounds for all points between $k = 0$ and $k = n$ is not obvious. A proof of this statement is provided in appendix A.

Since the time constant τ_m is a non-negative number, equation (22) implies that ξ_m must also satisfy the feasibility constraint

$$\xi_m \le 1 \tag{27}$$

in addition to the constraints given in equations (25) and (26).

When considering equations (24) through (27), it becomes clear that in order to upper bound σ_η^2, the following optimization problem must be solved for each sensor m.

$$\begin{aligned} \max_{r_{0,m},\,\xi_m} \quad & r_{0,m}\left(s_{0,m} + 2\sum_{k=1}^{n} s_{k,m}\,\xi_m^k\right) \\ \text{s.t.} \quad & a_{0,m} \le r_{0,m} \le b_{0,m} \\ & a_{n,m} \le r_{0,m}\,\xi_m^n \le b_{n,m} \\ & \xi_m \le 1 \end{aligned} \tag{28}$$

In the next section, a solution to this problem will be presented that involves polynomial root finding.

SOLUTION TO OPTIMIZATION PROBLEM

There are a total of five inequality constraints shown in equation (28), each of which defines a boundary curve in the $(r_{0,m}, \xi_m)$ plane.

Inequality Constraint	Boundary Equation
Number 1	$r_{0,m} = b_{0,m}$
Number 2	$r_{0,m}\,\xi_m^n = b_{n,m}$
Number 3	$\xi_m = 1$
Number 4	$r_{0,m} = a_{0,m}$
Number 5	$r_{0,m}\,\xi_m^n = a_{n,m}$

Table 1: Boundary equations for inequality constraints

When taken together, the equations shown in table 1 map out a feasible region for the optimization problem.

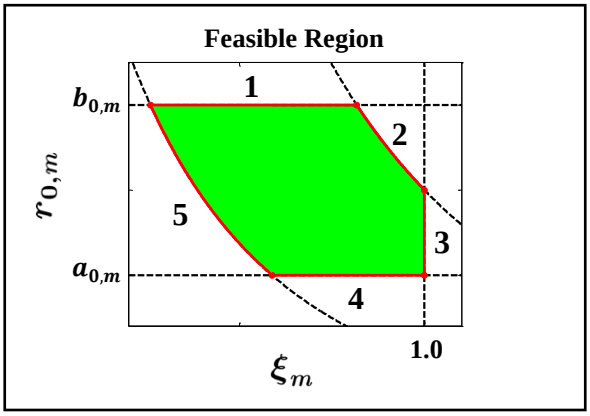

Figure 2: Feasible region for optimization problem

In general, the global optimum can exist in the interior or on the boundary of the feasible region. However, the cost function in equation (28) has a special structure which forces the global optimizer to be located on boundary curve 1 or 2. To see this, suppose that a stationary point $\left(r_{0,m}^{*}\,,\,\xi_{m}^{*}\right)$ has been found in the interior of the feasible region. Given the value ξ_{m}^{*}, the cost function can always be made larger by increasing $r_{0,m}^{*}$ until it reaches boundary curve 1 or 2. Therefore, solutions on these two boundaries only need to be considered.

Boundary Curve Number 1

Substituting $r_{0,m} = b_{0,m}$ into equation (28) results in the new optimization problem

$$\begin{aligned} \max_{\xi_m} \quad & b_{0,m}\left(s_{0,m} + 2\sum_{k=1}^{n} s_{k,m}\,\xi_m^{k} \right) \\ \text{s.t.} \quad & \left(\frac{a_{n,m}}{b_{0,m}}\right)^{1/n} \le \xi_m \le \left(\frac{b_{n,m}}{b_{0,m}}\right)^{1/n} \end{aligned} \tag{29}$$

Taking the derivative of the cost function with respect to ξ_m and setting the result equal to zero yields the polynomial equation

$$\sum_{k=1}^{n} k\, s_{k,m}\,\xi_m^{k-1} = 0 \tag{30}$$

The value of ξ_m which maximizes the cost function (denoted by $\xi_{m,1}^{*}$) must therefore be a root of this polynomial or one of the boundary points given in equation (29). The corresponding optimal value of $r_{0,m}$ (denoted by $r_{0,m,1}^{*}$) is simply given by $r_{0,m,1}^{*} = b_{0,m}$, because we are constrained to be on boundary curve 1.

Boundary Curve Number 2

Substituting $r_{0,m}\,\xi_m^{n} = b_{n,m}$ into equation (28) results in the new cost function

$$\max_{\xi_m} \quad \frac{b_{n,m}}{\xi_m^{n}}\left(s_{0,m} + 2\sum_{k=1}^{n} s_{k,m}\,\xi_m^{k} \right) \tag{31}$$

To determine the constraints on ξ_m, first recall from equation (25) that $a_{0,m} \le r_{0,m} \le b_{0,m}$. This inequality in conjunction with the equation for boundary curve 2 shown in table 1 implies that

$$\left(\frac{b_{n,m}}{b_{0,m}}\right)^{1/n} \le \xi_m \le \left(\frac{b_{n,m}}{a_{0,m}}\right)^{1/n} \tag{32}$$

However, ξ_m must also satisfy the constraint $\xi_m \le 1$. If $b_{n,m} > a_{0,m}$, then the upper bound in equation (32) will violate this constraint. Therefore, equation (32) must be modified to the form

$$\left(\frac{b_{n,m}}{b_{0,m}}\right)^{1/n} \le \xi_m \le \min\left[\left(\frac{b_{n,m}}{a_{0,m}}\right)^{1/n},\, 1 \right] \tag{33}$$

Equations (31) and (33) yield the following optimization problem along boundary curve 2.

$$\begin{aligned} \max_{\xi_m} \quad & \frac{b_{n,m}}{\xi_m^{n}}\left(s_{0,m} + 2\sum_{k=1}^{n} s_{k,m}\,\xi_m^{k} \right) \\ \text{s.t.} \quad & \left(\frac{b_{n,m}}{b_{0,m}}\right)^{1/n} \le \xi_m \le \min\left[\left(\frac{b_{n,m}}{a_{0,m}}\right)^{1/n},\, 1 \right] \end{aligned} \tag{34}$$

Taking the derivative of the cost function with respect to ξ_m and setting the result equal to zero yields the polynomial equation

$$n\,s_{0,m} + 2\sum_{k=1}^{n} (n-k)\, s_{k,m}\,\xi_m^{k} = 0 \tag{35}$$

The value of ξ_m which maximizes the cost function (denoted by $\xi_{m,2}^{*}$) must therefore be a root of this polynomial or one of the boundary points given in equation (34). The corresponding optimal value of $r_{0,m}$ (denoted by $r_{0,m,2}^{*}$) is obtained by substituting $\xi_{m,2}^{*}$ into the equation defining boundary curve 2. That is, $r_{0,m,2}^{*} = \left(\xi_{m,2}^{*}\right)^{-n}\, b_{n,m}$.

Given the two solutions $\left(r_{0,m,1}^{*}\,,\,\xi_{m,1}^{*}\right)$ and $\left(r_{0,m,2}^{*}\,,\,\xi_{m,2}^{*}\right)$, the global optimizer $\left(r_{0,m}^{*}\,,\,\xi_{m}^{*}\right)$ is that

point which produces the maximum value of the cost function given in equation (28).

Applying this procedure to each sensor m and substituting the global optimizers into equation (24) yields the following upper bound on σ_η^2.

$$\bar{\sigma}_\eta^2 = \sum_{m=1}^{M} r_{0,m}^* \left(s_{0,m} + 2\sum_{k=1}^{N-1} s_{k,m} \left(\xi_m^* \right)^k \right) \qquad (36)$$

APPLICATION TO CARRIER PHASE DIFFERENTIAL GPS

The theoretical development given thus far will now be applied to the problem of autonomous shipboard landing. An aircraft returning to the carrier must fly a specified flight pattern that is determined based on the current meteorological conditions. One example is a case-III approach, which is flown during adverse weather conditions and during all night flight operations. The approach is characterized by a series of precisely defined linear descent profiles. During the last two nautical miles (nmi), where integrity is critical, the aircraft descends at a constant speed of 150 knots on a 3.5° glideslope until touchdown as shown in figure 3.

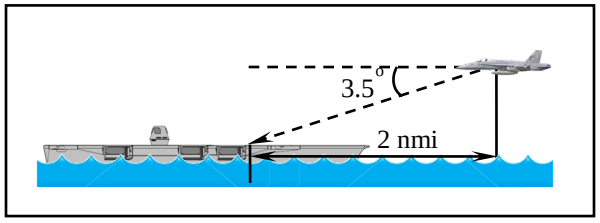

Figure 3: Final phase of case-III aircraft landing pattern

In order to achieve the necessary positioning accuracy, a dual frequency carrier phase differential GPS (CPDGPS) navigation algorithm is used to estimate $\Delta \boldsymbol{x}$. Given that the duration of the mission is very short, there is no significant change in satellite geometry to estimate the carrier phase cycle ambiguities. This in turn will affect the accuracy in the estimate of $\Delta \boldsymbol{x}$. One way to resolve this issue is to start the CPDGPS algorithm earlier, for example when the aircraft is 10 nmi from the ship. The major issue with this approach is the uncertainty in characterizing the ionospheric and tropospheric decorrelation errors. Unless these error sources can be faithfully modeled, the integrity of the entire navigation algorithm is at risk.

A second method to solve the observability problem is to use geometry-free prefiltering to estimate the widelane cycle ambiguities prior to arriving at the 2 nmi checkpoint. Because the geometry-free observable eliminates the ionospheric and tropospheric error sources, there are no potential integrity threats related to these errors. The prefiltering information is then used as prior knowledge to initialize the CPDGPS algorithm once the aircraft arrives at the 2 nmi checkpoint. The algorithm is depicted below in figure 4.

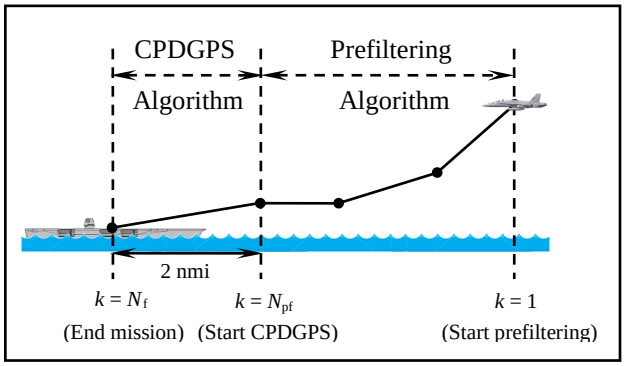

Figure 4: Algorithm description

N_{pf} is determined based on how long it takes the aircraft to arrive 2 nmi from the touchdown point. Unlike the aircraft, which has a definite mission duration, the carrier must be able to support a landing at any given time. Therefore, it is assumed that the ship begins prefiltering satellites as soon as they become visible.

GEOMETRY-FREE PREFILTERING

The geometry-free observable is defined as the difference between the widelane carrier and narrowlane pseudorange measurements.

$$z_{GF,k} = \phi_{WL,k} - \rho_{NL,k} \qquad (37)$$

$$\phi_{WL,k} = \frac{\lambda_{\text{L2}}}{\lambda_{\text{L2}} - \lambda_{\text{L1}}} \phi_{\text{L1},k} - \frac{\lambda_{\text{L1}}}{\lambda_{\text{L2}} - \lambda_{\text{L1}}} \phi_{\text{L2},k} \qquad (38)$$

$$\rho_{NL,k} = \frac{\lambda_{\text{L2}}}{\lambda_{\text{L1}} + \lambda_{\text{L2}}} \rho_{\text{L1},k} + \frac{\lambda_{\text{L1}}}{\lambda_{\text{L1}} + \lambda_{\text{L2}}} \rho_{\text{L2},k} \qquad (39)$$

where $\rho_{\text{L1},k}$, $\rho_{\text{L2},k}$, $\phi_{\text{L1},k}$ and $\phi_{\text{L2},k}$ are the raw L1 and L2 pseudorange and carrier phase measurements at epoch k in units of meters and λ_{L1}, λ_{L2} are the L1 and L2 carrier wavelengths.

It can be shown that this combination eliminates many terms in the GPS measurement model, including: receiver clock bias, satellite clock bias, ionospheric and tropospheric propagation delays and the user-to-satellite range. As a result, the measurement model for $z_{GF,k}$ has the simple form

$$z_{GF,k} = \frac{\lambda_{L1}\lambda_{L2}}{\lambda_{L2}-\lambda_{L1}}\left(n_{L1}-n_{L2}\right) + \nu_{GF,k} \qquad (40)$$

where n_{L1} and n_{L2} are the L1 and L2 carrier phase cycle ambiguities and $\nu_{GF,k}$ is the geometry-free measurement noise at epoch *k*, defined as

$$\begin{aligned}\nu_{GF,k} = b_1\nu_{\phi,L1,k} - b_2\nu_{\phi,L2,k} - \\ a_1\nu_{\rho,L1,k} - a_2\nu_{\rho,L2,k}\end{aligned} \qquad (41)$$

where, from equation (38), b_1 and b_2 are the coefficients in front of $\phi_{L1,k}$ and $\phi_{L2,k}$, respectively, and $\nu_{\phi,L1,k}$ and $\nu_{\phi,L2,k}$ are the time-correlated errors on the L1 and L2 carrier phase measurements at epoch *k*.

Similarly, from equation (39), a_1 and a_2 are the coefficients in front of $\rho_{L1,k}$ and $\rho_{L2,k}$, respectively, and $\nu_{\rho,L1,k}$ and $\nu_{\rho,L2,k}$ are the time-correlated errors on the L1 and L2 pseudorange measurements at epoch *k*.

Equation (40) can also be written in the form

$$\frac{z_{GF,k}}{\lambda_{WL}} = n_{WL} + \frac{1}{\lambda_{WL}}\nu_{GF,k} \qquad (42)$$

where $n_{WL} = n_{L1} - n_{L2}$ and λ_{WL} is the coefficient in front of $(n_{L1} - n_{L2})$ on the right hand side of equation (40).

As long as the GPS receiver maintains lock on the carrier signal, n_{WL} is a constant parameter that can be estimated using a simple averaging filter.

$$\hat{n}_{WL,k+1} = \frac{k}{k+1}\hat{n}_{WL,k} + \frac{1}{(k+1)\,\lambda_{WL}}z_{GF,k+1}$$
$$k = 0, 1, \cdots, N_{pf}-1 \qquad (43)$$

In appendix B, the following recursive expression is derived for the filtered estimate error variance.

$$\sigma^2_{pf,k+1} = 2\left(\frac{k}{k+1}\right)^2\sigma^2_{pf,k} - \left(\frac{k-1}{k+1}\right)^2\sigma^2_{pf,k-1} + \frac{2}{\lambda^2_{WL}(k+1)^2}r_{k_{GF}} \quad , \quad k = 1, 2, \cdots, N_{pf}-1$$
$$\sigma^2_{pf,1} = \frac{1}{\lambda^2_{WL}}r_{0_{GF}} \qquad (44)$$

where $r_{k_{GF}}$ is the value of the autocorrelation function of $\boldsymbol{\nu}_{GF}$ at a time shift of *k*.

The estimate $\hat{n}_{WL,N_{pf}}$ at the end of the prefiltering period can be viewed as a pseudo-measurement with the linear model

$$\hat{n}_{WL,N_{pf}} = n_{WL} + \nu_{pf,N_{pf}} \qquad (45)$$

where $\nu_{pf,N_{pf}}$ is the pseudo-measurement noise at the end of the prefiltering period which has the distribution

$$\nu_{pf,N_{pf}} \sim N\left(0, \sigma^2_{pf,N_{pf}}\right) \qquad (46)$$

and $\sigma^2_{pf,N_{pf}}$ is computed from equation (44).

CPDGPS NAVIGATION ALGORITHM

From the end of the prefiltering period until touchdown, the relative position vector is estimated using L1 and L2 double difference carrier phase measurements.

Since the main focus of this work is time-correlation uncertainty, simplified measurement models are used that do not include the effect of atmospheric propagation errors.

$$\Delta^2\phi^{ij}_{L1,k} = \boldsymbol{g}^T_{ij,k}\,\Delta\boldsymbol{x}_k + \lambda_{L1}\Delta^2 n^{ij}_{L1} + \Delta^2\nu^{ij}_{L1,k} \qquad (47)$$

$$\Delta^2\phi^{ij}_{L2,k} = \boldsymbol{g}^T_{ij,k}\,\Delta\boldsymbol{x}_k + \lambda_{L2}\Delta^2 n^{ij}_{L2} + \Delta^2\nu^{ij}_{L2,k} \qquad (48)$$

where $\Delta^2\phi^{ij}_{L1,k}$ and $\Delta^2\phi^{ij}_{L2,k}$ are the L1 and L2 double difference carrier phase measurements for satellites i and j at epoch *k*, $\boldsymbol{g}_{ij,k}$ is a column vector formed by differencing the line of sight unit vectors between satellites i and j at epoch *k* , $\Delta\boldsymbol{x}_k$ is the relative position

vector between the aircraft and ship at epoch k, $\Delta^2 n^{ij}_{L1}$ $\Delta^2 n^{ij}_{L2}$ are the L1 and L2 double difference cycle ambiguities for satellites i and j and $\Delta^2 \nu^{ij}_{L1,k}$, $\Delta^2 \nu^{ij}_{L2,k}$ are the time-correlated L1 and L2 double difference carrier phase measurement errors for satellites i and j at epoch k.

The double difference pseudo-measurement is combined with the current double difference carrier phase measurements to estimate $\Delta\boldsymbol{x}$ at the start of the CPDGPS algorithm.

Start of CPDGPS Algorithm: ($k = N_{pf}$)

$$\begin{bmatrix} \Delta^2 \hat{\boldsymbol{n}}_{WL} \\ \Delta^2 \boldsymbol{\phi}_{L1} \\ \Delta^2 \boldsymbol{\phi}_{L2} \end{bmatrix}_k = \begin{bmatrix} \mathbf{0} & \mathbf{I} & -\mathbf{I} \\ \mathbf{G} & \mathbf{I} & \mathbf{0} \\ \mathbf{G} & \mathbf{0} & \mathbf{I} \end{bmatrix}_k \begin{bmatrix} \Delta \boldsymbol{x}_k \\ \Delta^2 \boldsymbol{n}_{L1} \\ \Delta^2 \boldsymbol{n}_{L2} \end{bmatrix} + \begin{bmatrix} \Delta^2 \boldsymbol{\nu}_{pf} \\ \Delta^2 \boldsymbol{\nu}_{L1} \\ \Delta^2 \boldsymbol{\nu}_{L2} \end{bmatrix}_k \qquad (49)$$

where vector notation has been used to include all visible satellites and $\mathbf{G}$ is the geometry matrix whose rows are composed of all the available $\boldsymbol{g}^T_{ij,k}$'s .

It will be useful later on to write equation (49) as

$$\Delta^2 \boldsymbol{z}_k = \begin{bmatrix} \mathbf{H}_1 & \mathbf{H}_2 \end{bmatrix}_k \begin{bmatrix} \Delta \boldsymbol{x}_k \\ \Delta^2 \boldsymbol{n}_{L1} \\ \Delta^2 \boldsymbol{n}_{L2} \end{bmatrix} + \Delta^2 \boldsymbol{\nu}_k \qquad (50)$$

where $\mathbf{H}_1$ is the first column of the observation matrix in equation (49) and $\mathbf{H}_2$ is the last two columns of the observation matrix in equation (49). The definitions of $\Delta^2\boldsymbol{z}_k$ and $\Delta^2\boldsymbol{\nu}_k$ are obvious by comparing equations (49) and (50).

For all future epochs, L1 and L2 double difference carrier phase measurements are used to estimate $\Delta\boldsymbol{x}$.

CPDGPS Algorithm: $N_{pf} < k \le N_f$

$$\begin{bmatrix} \Delta^2 \boldsymbol{\phi}_{L1} \\ \Delta^2 \boldsymbol{\phi}_{L2} \end{bmatrix}_k = \begin{bmatrix} \mathbf{G} & \mathbf{I} & \mathbf{0} \\ \mathbf{G} & \mathbf{0} & \mathbf{I} \end{bmatrix}_k \begin{bmatrix} \Delta \boldsymbol{x}_k \\ \Delta^2 \boldsymbol{n}_{L1} \\ \Delta^2 \boldsymbol{n}_{L2} \end{bmatrix} + \begin{bmatrix} \Delta^2 \boldsymbol{\nu}_{L1} \\ \Delta^2 \boldsymbol{\nu}_{L2} \end{bmatrix}_k \qquad (51)$$

which can also be written as

$$\Delta^2 \boldsymbol{z}_k = \begin{bmatrix} \mathbf{H}_1 & \mathbf{H}_2 \end{bmatrix}_k \begin{bmatrix} \Delta \boldsymbol{x}_k \\ \Delta^2 \boldsymbol{n}_{L1} \\ \Delta^2 \boldsymbol{n}_{L2} \end{bmatrix} + \Delta^2 \boldsymbol{\nu}_k \qquad (52)$$

where $\mathbf{H}_1$ is the first column of the observation matrix in equation (51) and $\mathbf{H}_2$ is the last two columns of the observation matrix in equation (51). The definitions of $\Delta^2\boldsymbol{z}_k$ and $\Delta^2\boldsymbol{\nu}_k$ are obvious by comparing equations (51) and (52).

Measurements from epochs $k = N_{pf}$ to $k = N_{pf} + q$ are processed in a batch WLS estimator. The linear measurement model is given by

$$\begin{bmatrix} \Delta^2 \boldsymbol{z}_{N_{pf}} \\ \Delta^2 \boldsymbol{z}_{N_{pf}+1} \\ \vdots \\ \Delta^2 \boldsymbol{z}_{N_{pf}+q} \end{bmatrix} = \mathbf{H} \begin{bmatrix} \Delta \boldsymbol{x}_{N_{pf}} \\ \Delta \boldsymbol{x}_{N_{pf}+1} \\ \vdots \\ \Delta \boldsymbol{x}_{N_{pf}+q} \\ \Delta^2 \boldsymbol{n}_{L1} \\ \Delta^2 \boldsymbol{n}_{L2} \end{bmatrix} + \begin{bmatrix} \Delta^2 \boldsymbol{\nu}_{N_{pf}} \\ \Delta^2 \boldsymbol{\nu}_{N_{pf}+1} \\ \vdots \\ \Delta^2 \boldsymbol{\nu}_{N_{pf}+q} \end{bmatrix} \qquad (53)$$

where

$$\mathbf{H} = \begin{bmatrix} \mathbf{H}_{1,N_{pf}} & \mathbf{0} & \cdots & \mathbf{0} & \mathbf{H}_{2,N_{pf}} \\ \mathbf{0} & \mathbf{H}_{1,N_{pf}+1} & \cdots & \mathbf{0} & \mathbf{H}_{2,N_{pf}+1} \\ \vdots & \vdots & \ddots & \vdots & \vdots \\ \mathbf{0} & \mathbf{0} & \cdots & \mathbf{H}_{1,N_{pf}+q} & \mathbf{H}_{2,N_{pf}+q} \end{bmatrix} \qquad (54)$$

In its current form, the measurement noise vector in equation (53) is arranged according to time and not to satellite, which must be changed in order to comply with the form shown in equation (18). Furthermore, the double difference operation has introduced measurement error correlation across satellites which violates the assumption that measure errors are uncorrelated. These two discrepancies can be resolved through a linear transformation of the measurement noise vector.

The first step is to remove the double difference operation.

$$\begin{bmatrix} \Delta^2 \boldsymbol{\nu}_{N_{\mathrm{pf}}} \\ \Delta^2 \boldsymbol{\nu}_{N_{\mathrm{pf}}+1} \\ \vdots \\ \Delta^2 \boldsymbol{\nu}_{N_{\mathrm{pf}}+q} \end{bmatrix} = \mathbf{T}_d \begin{bmatrix} \Delta \boldsymbol{\nu}_{N_{\mathrm{pf}}} \\ \Delta \boldsymbol{\nu}_{N_{\mathrm{pf}}+1} \\ \vdots \\ \Delta \boldsymbol{\nu}_{N_{\mathrm{pf}}+q} \end{bmatrix} \tag{55}$$

where $\mathbf{T}_d$ is a block diagonal matrix with each block composed of the familiar double difference transformation matrix.

An additional transformation of equation (55) is performed to arrange the single difference measurement noise vector according to satellite.

$$\begin{bmatrix} \Delta \boldsymbol{\nu}_{N_{\mathrm{pf}}} \\ \Delta \boldsymbol{\nu}_{N_{\mathrm{pf}}+1} \\ \vdots \\ \Delta \boldsymbol{\nu}_{N_{\mathrm{pf}}+q} \end{bmatrix} = \mathbf{T}_s \begin{bmatrix} \Delta \boldsymbol{\nu}_1 \\ \Delta \boldsymbol{\nu}_2 \\ \vdots \\ \Delta \boldsymbol{\nu}_M \end{bmatrix} \tag{56}$$

where $\mathbf{T}_s$ is a matrix of 0's and 1's, M is the total number of visible satellites and each of the $\Delta\boldsymbol{\nu}_m$'s has the following structure

$$\Delta \boldsymbol{\nu}_m = \begin{bmatrix} \Delta \nu_{m,\mathrm{pf}} & \Delta \boldsymbol{\nu}_{m,\mathrm{L1}}^T & \Delta \boldsymbol{\nu}_{m,\mathrm{L2}}^T \end{bmatrix}^T \tag{57}$$

where $\Delta\nu_{m,\mathrm{pf}}$ is the single difference prefiltering error for satellite m at $k = N_{\mathrm{pf}}$, $\Delta\boldsymbol{\nu}_{m,\mathrm{L1}}$ is a time series of the single difference L1 carrier phase measurement error for satellite m from $k = N_{\mathrm{pf}}$ to $k = N_{\mathrm{pf}} + q$ and $\Delta\boldsymbol{\nu}_{m,\mathrm{L2}}$ is a time series of the single difference L2 carrier phase measurement error for satellite m from $k = N_{\mathrm{pf}}$ to $k = N_{\mathrm{pf}} + q$.

Combining the two transformation matrices in equations (55) and (56) in one matrix **J** yields

$$\mathbf{J} = \mathbf{T}_d \, \mathbf{T}_s \tag{58}$$

which allows equation (53) to be written as

$$\begin{bmatrix} \Delta^2 \boldsymbol{z}_{N_{\mathrm{pf}}} \\ \Delta^2 \boldsymbol{z}_{N_{\mathrm{pf}}+1} \\ \vdots \\ \Delta^2 \boldsymbol{z}_{N_{\mathrm{pf}}+q} \end{bmatrix} = \mathbf{H} \begin{bmatrix} \Delta \boldsymbol{x}_{N_{\mathrm{pf}}} \\ \Delta \boldsymbol{x}_{N_{\mathrm{pf}}+1} \\ \vdots \\ \Delta \boldsymbol{x}_{N_{\mathrm{pf}}+q} \\ \Delta^2 \boldsymbol{n}_{\mathrm{L1}} \\ \Delta^2 \boldsymbol{n}_{\mathrm{L2}} \end{bmatrix} + \mathbf{J} \begin{bmatrix} \Delta \boldsymbol{\nu}_1 \\ \Delta \boldsymbol{\nu}_2 \\ \vdots \\ \Delta \boldsymbol{\nu}_M \end{bmatrix} \tag{59}$$

Assuming that measurement errors are uncorrelated across satellites, $\mathbf{P}_\nu$ is a block diagonal matrix with each block given by

$$\mathbf{P}_{\nu,m} = \begin{bmatrix} \sigma^2_{\Delta\nu_{m,\mathrm{pf}}} & \mathbf{0} & \mathbf{0} \\ \mathbf{0} & \mathbf{P}_{\Delta\nu_{m,\mathrm{L1}}} & \mathbf{0} \\ \mathbf{0} & \mathbf{0} & \mathbf{P}_{\Delta\nu_{m,\mathrm{L2}}} \end{bmatrix} \tag{60}$$

From equation (41) it can be seen that $\nu_{GF,k}$ is partially composed of $\nu_{\phi,\mathrm{L1},k}$ and $\nu_{\phi,\mathrm{L2},k}$. This implies that $\sigma^2_{\mathrm{pf},N_{\mathrm{pf}}}$ computed in equation (44) is correlated with all past, present and future values of $\nu_{\phi,\mathrm{L1},k}$ and $\nu_{\phi,\mathrm{L2},k}$. Therefore, the two zero matrices in the first row and first column of $\mathbf{P}_{\nu,m}$ are in fact non-zero. However, it can be shown that the approximate form given in equation (60) results in a conservative estimate error variance, and so this correlation will not be considered here.

In the next section, a numerical simulation will be conducted to demonstrate the feasibility of the bounding algorithm developed in this work. Furthermore, it will be shown that larger time constants do not always produce an upper bound on the estimate error variance.

NUMERICAL SIMULATION RESULTS

A batch WLS estimator can be applied to the linear model shown in equation (59) using the simulation parameters summarized below in table 2.

Simulation Parameter	Assigned Value
GPS sampling interval	T = 1.0 sec
Satellite constellation	May 2007 almanac (30 SVs)
Simulation location	Off the coast of California
Prefiltering duration	N_{pf} = 600
Mission duration	N_{f} = 900

Table 2: Simulation parameters

At first glance, it appears from equation (60) that autocorrelation bounds must be defined for three measurement error sources per satellite: single difference geometry-free measurement error and L1, L2 single difference carrier phase measurement errors. However, the geometry-free measurement error can be characterized separately for the aircraft and ship. Therefore, four autocorrelation bounds will be defined for each satellite.

Recall from equation (43) that the geometry-free prefiltering algorithm is a simple averaging filter. In this case, it is already known a priori that more measurement error correlation will produce a conservative estimate error variance. Hence, only an upper bound on the geometry-free measurement error autocorrelation function is required.

Measurement Error	Autocorrelation Lower Bound	Autocorrelation Upper Bound
Aircraft geometry-free	N/A	$b_0 = 13\ \text{cm}^2$ $\tau_b = 50\ \text{sec}$
Ship geometry-free	N/A	$b_0 = 13\ \text{cm}^2$ $\tau_b = 100\ \text{sec}$
L1/L2 SD carrier phase	$a_0 = 2\ \text{cm}^2$ $\tau_a = 50\ \text{sec}$	$b_0 = 2\ \text{cm}^2$ $\tau_b = 150\ \text{sec}$

Table 3: Autocorrelation bounds

There are two important aspects worth mentioning about the autocorrelation bounds shown in table 3. First, one set of bounds has been defined that will be applied to all satellites and no attempt has been made to define individual autocorrelation bounds. The second aspect is that the measurement noise variance is assumed to be known precisely, which is why $a_0 = b_0$ for the L1/L2 single difference carrier phase measurement error bounds. Of course, this assumption is not necessary to use the algorithms developed earlier and was simply made to reduce the number of varying parameters.

Using the vertical component of the relative position estimate error vector as an example, the true estimate error variance and associated upper bound can be computed using equations (13) and (36), respectively.

$$\sigma_v^2 = \boldsymbol{\alpha}_v^T \hat{\mathbf{S}} \mathbf{J} \mathbf{P}_\nu \mathbf{J}^T \hat{\mathbf{S}}^T \boldsymbol{\alpha}_v \qquad (61)$$

$$\bar{\sigma}_v^2 = \sum_{m=1}^{M} r_{0,m}^* \left(s_{0,m} + 2 \sum_{k=1}^{N-1} s_{k,m} \left(\xi_m^* \right)^k \right) \qquad (62)$$

In this work, the pseudoinverse $\hat{\mathbf{S}}$ is populated using the values corresponding to the upper bounding functions shown in table 3.

Measurement Error	Estimator Model
Aircraft geometry-free	$r_0 = 13\ \text{cm}^2$ $\hat{\tau} = 50\ \text{sec}$
Ship geometry-free	$r_0 = 13\ \text{cm}^2$ $\hat{\tau} = 100\ \text{sec}$
L1/L2 SD carrier phase	$r_0 = 2\ \text{cm}^2$ $\hat{\tau} = 150\ \text{sec}$

Table 4: Measurement noise models used in estimator

The ultimate goal is to verify that $\bar{\sigma}_v^2 \geq \sigma_v^2$ for all measurement noise characteristics (within the allowable bounds) that may be encountered in nature. Clearly, this cannot be accomplished due to computational limitations. However, we can verify that this statement is true for a finite set of true measurement noise scenarios.

Three different scenarios will be considered here, and are summarized below in table 5.

Truth Scenario	Truth Characteristics
Scenario 1	$\tau_{\text{true}} = [40 \quad 90 \quad 120]\ \text{sec}$
Scenario 2	$\tau_{\text{true}} = [45 \quad 95 \quad 120]\ \text{sec}$
Scenario 3	$\tau_{\text{true}} = [50 \quad 100 \quad 120]\ \text{sec}$

Table 5: True measurement noise characteristics

To illustrate what the numbers mean in table 5, consider scenario 1. The true aircraft geometry-free measurement error time constant is 40 sec, the true ship geometry-free measurement error time constant is 90 sec and the true L1/L2 single difference carrier phase measurement error time constant is 120 sec.

These values are applied as a truth model to populate $\mathbf{P}_\nu$ in equation (61) for all visible satellites.

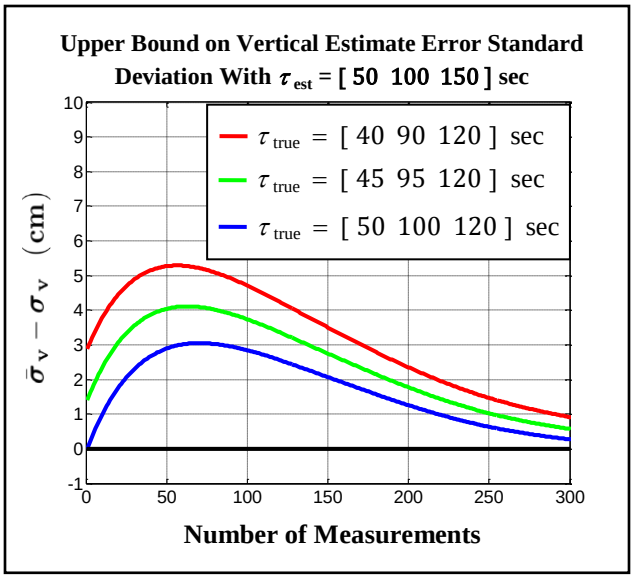

Figure 5: Bounding results for vertical estimate error

Notice that the y-axis in figure 5 is the difference between the bounding standard deviation computed from equation (62) and the true standard deviation computed using equation (61). The fact that this difference is positive for all three truth scenarios shows that the bounding algorithm does indeed result in an upper bound on the true estimate error standard deviation.

It is also interesting to see what values of ξ_m^* produced the bound in equation (62). Since the time constant τ_m is more intuitively appealing than ξ_m, the bounding value τ_m^* will be presented in place of ξ_m^*.

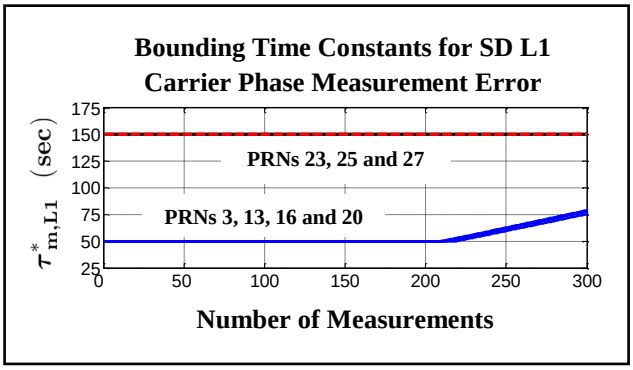

Figure 6: Bounding time constant on SD L1 carrier phase measurement error

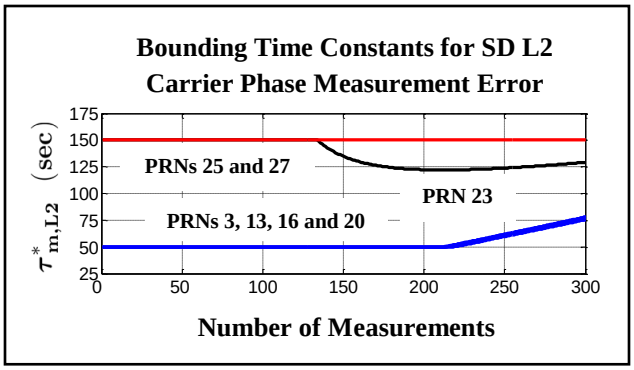

Figure 7: Bounding time constant on SD L2 carrier phase measurement error

One way to view the results shown in figures 6 and 7 is that if $\mathbf{P}_v$ were populated using these values for the time constant, then the true estimate error variance computed in equation (61) would achieve its maximum value, i.e. $\sigma_v^2 = \bar{\sigma}_v^2$. As an example, suppose that 50 measurements are processed in the batch WLS estimator. Then the worst possible measurement noise scenario would occur when PRNs 3, 13, 16 and 20 have a time constant of 50 seconds and PRNs 23, 25 and 27 have a time constant of 150 seconds on both the L1 and L2 frequencies. Even more profound is the fact that this situation will produce a larger estimate error variance than the situation in which all satellites have a time constant of 150 sec. Therefore, choosing a larger time constant does not necessarily guarantee an upper bound on the estimate error variance and we cannot ensure integrity.

Not only is the bounding time constant different for each visible satellite, but it also changes as more and more measurements are processed in the batch estimator. PRNs 3, 13, 16 and 20 remain at the lower time constant until approximately 210 measurements are reached. At this point, satellite motion begins to take effect and the bounding time constant slowly starts to rise. PRN 23 also exhibits such behavior on the L2 frequency. These results provide justification that no heuristic arguments can be made to conservatively model time-correlated measurement noise.

CONCLUSION

In this paper, a methodology was developed to upper bound fault-free integrity risk in the presence of time correlation uncertainty. For measurement noise distributions described by a first order Gauss-Markov model, the estimate error variance was expressed directly

in terms of the variance and time constant defining the process. Provided that the autocorrelation function can be bounded above and below by specified exponential functions, an upper bound on the estimate error variance can be obtained using polynomial root finding. Applying this method to the benchmark application of autonomous shipboard landing, it was shown that the algorithm developed in this work does indeed upper bound the true estimate error variance for three truth scenarios. Furthermore, it was shown that the bounding time constant can vary across satellites and changes with time due to the effect of satellite motion.

In any practical situation, it will be next to impossible to verify that the measurement noise is exactly described by a first order Gauss-Markov model. Therefore, future studies will focus on generalizing the bounding algorithms developed in this work to situations where the measurement noise does not have a prescribed mathematical form. In addition, the vast majority of estimators that process measurements over time are recursive in nature. The most well known is the Kalman filter. If the algorithms developed in this work are to be generally useful, they must be applicable to recursive estimators. This generalization will also be a primary focus in future studies of bounding integrity risk in the presence of time-correlation uncertainty.

ACKNOWLEDGEMENTS

We would like to gratefully acknowledge our research sponsors at Navair and L3 Communications. Without their continued support, this research would not have been possible.

REFERENCES

[1] B. DeCleene, *Defining Pseudorange Integrity – Overbounding*, Proceedings of the Institute of Navigation's ION-GPS 2000, pp. 1916 – 1924.

[2] J. Rife, S. Pullen, B. Pervan, and P. Enge, *Paired Overbounding and Application to GPS Augmentation*, IEEE Position, Location and Navigation Symposium, pp. 439-446, 2004.

[3] J. Rife and D. Gebre-Egziabher, *Symmetric Overbounding of Correlated Errors*, NAVIGATION, 2007, Vol. 54, No. 2, pp. 109-124.

[4] G.W. Pulford, *A Proof of the Spherically Symmetric Overbounding Theorem for Linear Systems*, NAVIGATION, 2008, Vol. 55, No. 4, pp. 283-292.

[5] S. Khanafseh, S. Langel and B. Pervan, *Overbounding Position Errors in the Presence of Carrier Phase Multipath Error Model Uncertainty*, IEEE/ION Position, Location and Navigation Symposium, 2010, pp. 575-584.

[6] Simon, Dan. Optimal State Estimation: Kalman, H-infinity and Nonlinear Approaches. New Jersey: John Wiley and Sons, Inc., 2006.

[7] Gelb, Arthur. Applied Optimal Estimation. The Analytic Sciences Corporation, 1974.

[8] Schneider, Hans. Matrices and Linear Algebra New York: Holt, Rinehart and Winston, Inc., 1968.

APPENDIX A

This appendix is concerned with exponential autocorrelation functions that are bounded above and below by predefined exponential functions, as shown below in figure 1A.

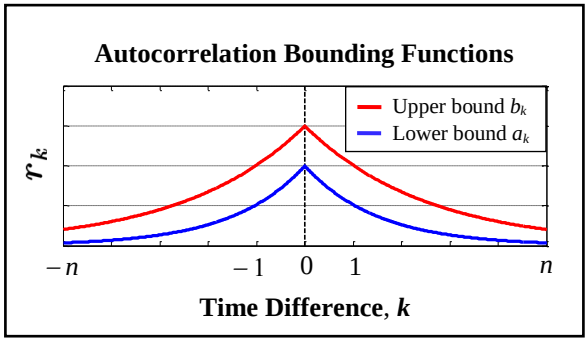

Figure 1A: Autocorrelation uncertainty structure

It will be shown that any candidate autocorrelation function r_k whose value at $k = 0$ and $k = n$ lies between the specified bounds must lie between the bounds for all values of k between 0 and n.

The autocorrelation function, r_k, has the following form

$$r_k = r_0 \, \xi^k \tag{1A}$$

where

$$\xi = \exp\left(-\frac{T}{\tau} \right) \tag{2A}$$

The two bounding functions a_k and b_k shown in figure 1A have a similar form.

$$a_k = a_0 \xi_a^k \tag{3A}$$

$$b_k = b_0 \xi_b^k \tag{4A}$$

Suppose that r_k is known to lie between the two bounding functions at $k = 0$ and $k = n$.

$$a_0 \le r_0 \le b_0 \tag{5A}$$

$$a_n \le r_0 \xi^n \le b_n \tag{6A}$$

With the aid of equations (3A) and (4A), equation (6A) can also be written as

$$\left(\frac{a_0}{r_0} \right) \xi_a^n \le \xi^n \le \left(\frac{b_0}{r_0} \right) \xi_b^n \tag{7A}$$

which, for $n > 0$, can be expressed as

$$\left(\frac{a_0}{r_0} \right)^{1/n} \xi_a \le \xi \le \left(\frac{b_0}{r_0} \right)^{1/n} \xi_b \quad , \quad n > 0 \tag{8A}$$

Proof that $r_k \ge a_k$ for all $k \in (0, n)$

This statement can be proved by contradiction. Suppose that r_k drops below a_k for some $k \in (0, n)$.

$$r_0 \xi^k < a_0 \xi_a^k \quad , \quad k \in (0, n) \tag{9A}$$

Equation (9A) implies that

$$\xi < \left(\frac{a_0}{r_0} \right)^{1/k} \xi_a \quad , \quad k \in (0\,,\, n) \tag{10A}$$

When taken together with the lower bound in equation (8A), we obtain the inequality

$$\left(\frac{a_0}{r_0} \right)^{1/n} \xi_a \le \xi < \left(\frac{a_0}{r_0} \right)^{1/k} \xi_a \ , \ k \in (0\,,\, n) \tag{11A}$$

which can simplified to the form

$$\left(\frac{a_0}{r_0} \right)^{\frac{1}{n} - \frac{1}{k}} \le \xi < 1 \ , \ k \in (0\,,\, n) \tag{12A}$$

However, because $a_0 \le r_0$ and $k < n$, we know that

$$\left(\frac{a_0}{r_0} \right)^{\frac{1}{n} - \frac{1}{k}} > 1 \quad , \quad k \in (0\,,\, n) \tag{13A}$$

This contradicts the inequality in equation (12A) and therefore the inequality in equation (9A) cannot be true. Hence, the conditions shown in equations (5A) and (6A) guarantee that r_k will never drop below the lower bounding function, a_k.

Proof that $r_k \le b_k$ for all $k \in (0, n)$

Now suppose that r_k rises above b_k for some $k \in (0, n)$.

$$r_0 \xi^k > b_0 \xi_b^k \quad , \quad k \in (0, n) \tag{14A}$$

Equation (14A) implies that

$$\xi > \left(\frac{b_0}{r_0} \right)^{1/k} \xi_b \quad , \quad k \in (0\,,\, n) \tag{15A}$$

When taken together with the upper bound in equation (8A), we obtain the inequality

$$\left(\frac{b_0}{r_0} \right)^{1/k} \xi_b < \xi \le \left(\frac{b_0}{r_0} \right)^{1/n} \xi_b \ , \ k \in (0\,,\, n) \tag{16A}$$

which can be simplified to the form

$$1 \le \xi \le \left(\frac{b_0}{r_0} \right)^{\frac{1}{n} - \frac{1}{k}} \ , \ k \in (0\,,\, n) \tag{17A}$$

However, because $b_0 \ge r_0$ and $k < n$, we know that

$$\left(\frac{b_0}{r_0} \right)^{\frac{1}{n}-\frac{1}{k}} < 1 \quad , \quad k \in (0\,,\,n) \tag{18A}$$

This contradicts the inequality in equation (17A) and therefore the inequality in equation (14A) cannot be true. Hence, the conditions shown in equations (5A) and (6A) guarantee that r_k will never rise above the upper bounding function, b_k.

APPENDIX B

In this appendix, a recursive expression will be derived for the estimate error variance associated with a simple averaging filter. The measurement model is given by

$$z_k = x + \nu_k \tag{1B}$$

where z_k is the measurement at time k, x is a constant parameter to be estimated and ν_k is the measurement noise at time k.

The unknown parameter x is estimated using a simple averaging filter. With one measurement available, the estimate and associated estimate error are given by

$$\hat{x}_1 = z_1 \tag{2B}$$

Substituting equation (1B) into equation (2B) yields

$$\hat{x}_1 = x + \nu_1 \tag{3B}$$

From which we can obtain the estimate error and associated estimate error variance

$$\varepsilon_1 = \hat{x}_1 - x = \nu_1 \tag{4B}$$

$$\sigma_1^2 = r_0 \tag{5B}$$

where r_0 is value of the autocorrelation function of ν_k at a time shift of 0.

With two measurements, x is estimated via

$$\hat{x}_2 = \frac{1}{2}\left(z_1 + z_2 \right) \tag{6B}$$

Substituting equation (1B) into equation (6B) results in

$$\hat{x}_2 = \frac{1}{2}\left(x + \nu_1 + x + \nu_2 \right) \tag{7B}$$

which yields the estimate error

$$\varepsilon_2 = \frac{1}{2}\left(\nu_1 + \nu_2 \right) \tag{8B}$$

Evaluating the expected value of ε_2^2 gives the estimate error variance

$$\sigma_2^2 = \frac{1}{4}\left(2r_0 + 2r_1 \right) \tag{9B}$$

We can continue in this fashion to determine the estimate error variance at any arbitrary epoch. For convenience, the first four values of the estimate error variance are shown below.

$$\sigma_1^2 = r_0 \tag{10B}$$

$$\sigma_2^2 = \frac{1}{2}r_0 + \frac{1}{2}r_1 \tag{11B}$$

$$\sigma_3^2 = \frac{1}{3}r_0 + \frac{4}{9}r_1 + \frac{2}{9}r_2 \tag{12B}$$

$$\sigma_4^2 = \frac{1}{4}r_0 + \frac{6}{16}r_1 + \frac{4}{16}r_2 + \frac{2}{16}r_3 \tag{13B}$$

After working with equations (10B) through (13B), the following recursive expression can be derived

$$\sigma_k^2 = 2\left(\frac{k-1}{k} \right)^2 \sigma_{k-1}^2 - \left(\frac{k-2}{k} \right)^2 \sigma_{k-2}^2 + \frac{2}{k^2} r_{k-1} \quad , \quad k = 2\,,\,3\,,\cdots \tag{14B}$$

$$\sigma_1^2 = r_0$$